CONF-801124--19

CHARACTERIZATION OF IRON-ENRICHED SYNTHETIC BASALT FOR TRANSURANIC CONTAINMENT

MASTER

by

J. E. Flinn
S. P. Henslee
P. V. Kelsey
R. L. Tallman
J. M. Welch

Materials Technology Division
EG&G Idaho, Inc., Idaho Falls, ID

October 17, 1980

Submitted to Materials Research Society
For Presentation and Proceedings Publication
on the Symposia for Scientific Basis for
Nuclear Waste Management, Boston, Mass.,
November 17 - 21, 1980.

CHARACTERIZATION OF IRON-ENRICHED SYNTHETIC BASALT FOR TRANSURANIC CONTAINMENT

J. E. Flinn, S. P. Henslee, P. V. Kelsey,
R. L. Tallman, and J. M. Welch

Materials Technology Division, EG&G Idaho Inc.
P. O. Box 1625, Idaho Falls, ID 83415

INTRODUCTION

Considerable quantities of low-level and transuranic (TRU) wastes are being temporarily stored at Idaho National Engineering Laboratory (INEL). Estimates show that stored and buried wastes at INEL will approach 4×10^5 m^3 by 2000 AD. Main combustible components of INEL waste forms are paper, wood, and plastics, and main noncombustibles are concrete, metals, sludge, and soil. Two prime benefits realizable by solidification are: (a) substantial volume reduction is achieved and (b) stabilized waste forms are suitable for either short- or long-term storage.

Slagging pyrolytic incineration (SPI) is being considered to convert stored and buried wastes into a slag.[1] In this process, combustibles are burned and noncombustibles, including metals, are oxidized into a molten slag, with further processing conducted in a heated tundish, e.g., an electromelter, where the molten slag is allowed to homogenize (within a reasonable time period) and then cast into large, cylindrical metal containers. Analyses of INEL waste slags[2] show them similar in composition and appearance to natural basalts, but rich in iron.

Most of the characterization assessments of synthetic slag wastes have been run on small melts, which are highly vitreous and were not representative of castings that normally result from a combined SPI-tundish process. Penberthy Electromelt of Seattle, Washington, produced 90-kg slag castings with compositions approximating average INEL waste as well as average wastes containing various amounts of soil from the INEL site.

In total, four melts and subsequent castings were made. This paper summarizes the evaluation of these castings.

MELTING AND CASTING

Large-scale castings were made for four compositions (representing the major oxide components associated with average waste with various soil additions[2]) using an electromelt process. The melt batches were premixed from industrial grade powders and soil, where applicable. The charge was usually completed in one day, and the melter held at 1300 to 1480°C overnight, with pouring usually accomplished the next day. The canisters used to contain the molten slag through subsequent cooling were galvanized steel and/or mild steel, 38.1 cm in diameter x 43.2 cm high x 0.18 cm thick.

Before pouring, the bottoms of three canisters used in the initial tests were filled 2.5-cm deep with sand for insulating purposes. Furthermore, two small holes were drilled into the bottom of each canister to vent air and steam from the sand layer. The fourth casting was cooled via a 7.6-cm thick steel plate placed under the canister for heat extraction. All canisters effectively contained their melts.

GENERAL STRUCTURAL FEATURES

The overall appearance of the interiors of castings was rock-like. In general, the texture or grain size near canister walls was finer than that near the center of the castings. The overall grain size for castings is considerably finer than that observed for natural basalt in Idaho. This is expected since cooling of these castings was considerably faster (less than 24 hrs from pouring temperature to room temperature) than the cooling of most natural basalts.

The castings each displayed a friable crust and a center cavity. The crust probably was due to a faster cooling rate on the surface than in the interior since it was directly exposed to air. This exposure would also promote thermal shock. The porous cavity represented approximately 10 percent of the total casting volume.

Plugs from various locations within the castings were removed by core drilling. The plugs were sectioned into discs, then analyzed and tested. By chemical analysis, each casting was homogeneous. The nominal compositions are shown in Table 1. The most notable difference for the series is the A-30 casting, with exceptionally high iron content and ferrous-to-ferric iron ratio.

TABLE 1. Nominal Chemical Composition of A-Series Electromelt Slags

Slag	Oxide Compounds (wt/%)								
	SiO_2	Al_2O_3	Fe_2O_3	FeO	TiO_2	CaO	MgO	K_2O	Na_2O
A-0	40.4	10.2	15.6	14.8	0.07	8.6	3.4	1.8	5.0
A-20	42.9	10.6	9.8	15.8	0.30	10.8	3.3	1.9	4.4
A-30	47.8	11.0	2.5	19.6	0.24	9.6	2.9	2.1	4.2
A-40	51.3	11.0	6.1	11.7	0.05	9.8	2.4	1.7	6.0

PHASE AND MICROSTRUCTURE

Crystalline phases present in the A-series slags are augite, magnetite, and probably hematite (in some areas) as determined by X-ray diffraction, microscopic examination, and EDS analysis.

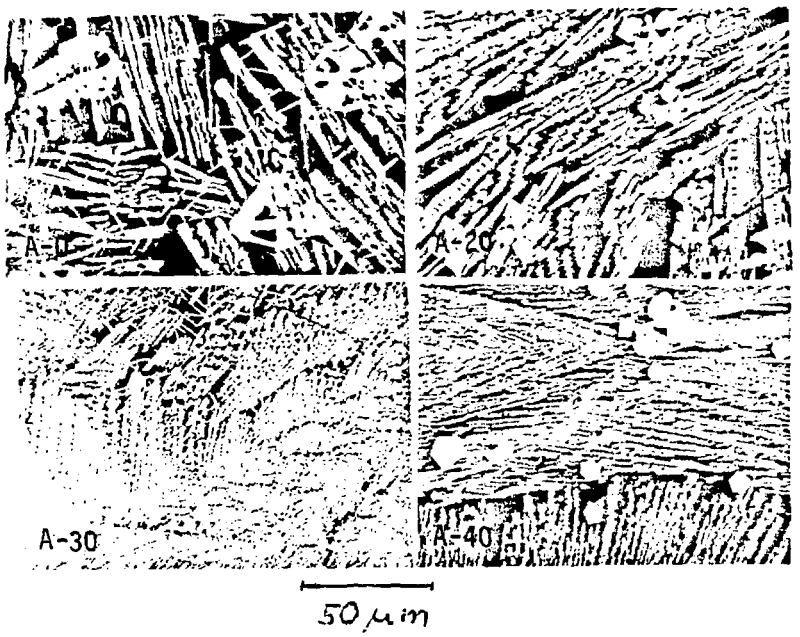

Figure 1. Photomicrographs of A-series slags. All samples were taken from the upper middle sections of the castings and their chemical compositions are shown in Table 1.

The microstructure of the A-0 casting, shown in Figure 1, is feathered acicular augite (light gray regions) with large spinel dendrites (white regions within the matrix). The darker gray area (matrix) is glass.

The microstructure of A-20 specimens (Figure 1), is similar to that of the A-0 casting except that there is less spinel and the augite crystals are slightly larger. The microstructures of the bulk of the A-30 specimens (Figure 1) are dominated by two phases, fine-acicular augite and glass; very little spinel was observed. The microstructure of A-40 specimens shows a marked decrease in the amount of spinel present (Figure 1). However, the A-30 specimen taken near the air-exposed surface showed typical levels of spinel, augite, and glass when compared to A-0 and A-40 structures.

Results show that a) number and size of the spinel grains decrease with decreasing total iron and/or Fe_2O_3 contents and b) the degree of devitrification increases and grain size decreases with increasing ratios of silica to iron oxides.

LEACHING

Rectangular-shaped monoliths (2.3 to 2.9 g) for leaching assessments were sectioned from plug cores. The monoliths were abraded and polished, cleaned, and weighed on a microbalance, then suspended in 70°C deionized water for 14 d. The volume of leachant was 40 ml/cm^2 of specimen surface. Results were determined from weight loss measurements, and from leachant analyses by emission spectroscopy.

The results are shown in Table 2. The agreement between the two measurements is very good. The leach rates range from 30×10^{-6} $g/cm^2 \cdot d$ for A-0 to 8×10^{-6} $g/cm^2 \cdot d$ for A-40 slags. These values are ten to thirty times higher than those reported for more vitreous melt specimens.[2]

The normalized compositions of the leachates were about the same for all leach specimens from the four castings. The leached composition was 47 w/o SiO_2, 29 w/o Na_2O, 18 w/o Al_2O_3, 5 w/o K_2O, 0.6 w/o CaO, 0.3 w/o Fe_2O_3, and 0.3 w/o MgO. This composition seems to be a derivative from the glass regions of the slags with very little contribution from either the diopside solid-solution or spinel phases.

Leach rates (Table 2) increased with increasing iron and decreasing silica content, and with increasing glass-phase content. Microcracking increased with iron content, increasing the surface area available for leaching. A high pH from the dissolution of alkali in a crack can promote the dissolution of

TABLE 2. LEACHING RESULTS FOR ELECTROMELT SLAG SPECIMENS
(14 day Static Test at 70°C)

Slag Type	Specimen No.	Surface Area (cm^2)	Weight Loss (mg)	Leach Rate ($\mu g/cm^2 \cdot d$)	Total Oxidea Leach Rate ($\mu g/cm^2 \cdot d$)
A-20	1	5.730	1.500	18.7	19.8
	2	5.768	1.719	21.3	22.0
	3	5.582	1.825	22.6	26.4
A-40	4	5.969	0.650	7.8	10.8
	5	5.381	0.749	9.9	13.1
	6	5.618	0.704	9.0	11.3
A-30	7	5.204	1.089	14.9	17.8
	8	5.732	1.360	16.9	20.2
	9	5.215	1.086	14.9	18.8
	10	5.599	0.968	12.3	15.8
A-0	11	5.553	2.764	35.6	38.0
	12	5.652	2.616	33.1	37.2
	13	5.730	1.042	13.0	17.7

a. From leachant analyses, converted to oxides.

Al_2O_3 and SiO_2. Dissolution could be further enhanced at crack tips by the presence of high tensile stresses.

MECHANICAL BEHAVIOR

Mechanical property measurements were obtained on the slag specimens; these included splitting tensile strengths (ASTM 496-71), fracture toughness, and diamond pyramid microhardness. In addition to the hardness values, the extent and nature of the microcracks from six indentation load levels also were determined.

The splitting tensile strengths and fracture toughness values determined on the plug samples removed from the castings are shown in Table 2. A-20 appears to be slightly stronger than either A-0 or A-30. This behavior can be explained in part by analysis of the failed specimens. The fracture surfaces

produced from the tests for A-0 and A-30 are similar in surface roughness and general appearance, while the failed surface of the A-20 was less coarse. The implication is that the A-20 contained a higher density of micro-cracks and thus required more energy to propagate those micro-cracks. This assumption is reinforced by the size of the particles produced by the splitting tensile test. The A-20 produced a noticeably finer particle, generating more surface area than either A-0 or A-30, and thus requiring more energy.

Fracture toughness values (Table 3) for the slags were lower than for the borosilicate glass. This can be explained again by the relative amount of micro-cracking exhibited by the various samples. The borosilicate glass showed no visible signs of micro-cracking while all three slags were extensively micro-cracked. The presence of micro-cracks could be considered advantageous with respect to fracture toughness through multiple crack paths etc., but this is not necessarily the case since the toughness values for the slags do not correlate to the amount of micro-cracking. All else being equal, the borosilicate glass should exhibit greater fracture toughness values since there was no micro-cracking. The effect of micro-cracking should be noticeable in the crack propagation rate where multiple crack paths and crack branching play an important role and would subsequently decrease the rate.

Microhardness of spinel phases was identical to that of the remaining matrix. Measured microcrack lengths produced by indentations (Figure 2), showed no apparent correlation with phases present, i.e., a preference for the microcracks to follow phase boundaries rather than crossing phases was not seen.

TABLE 3. SPLITTING TENSILE STRENGTH AND FRACTURE TOUGHNESS RESULTS

	Splitting Tensile, MPa		Fracture Toughness, MPa $\sqrt{m}$	
Slag Type	Strength	Std. Deviation	K_{Ic}^{SR}	Std. Deviation
A-0	13.23	3.92	0.92	0.13
A-20	16.02	5.56	0.95	0.06
A-30	12.65	3.53	1.13	0.20
Borosilicate Glass	43.3	14.39	1.41	0.09

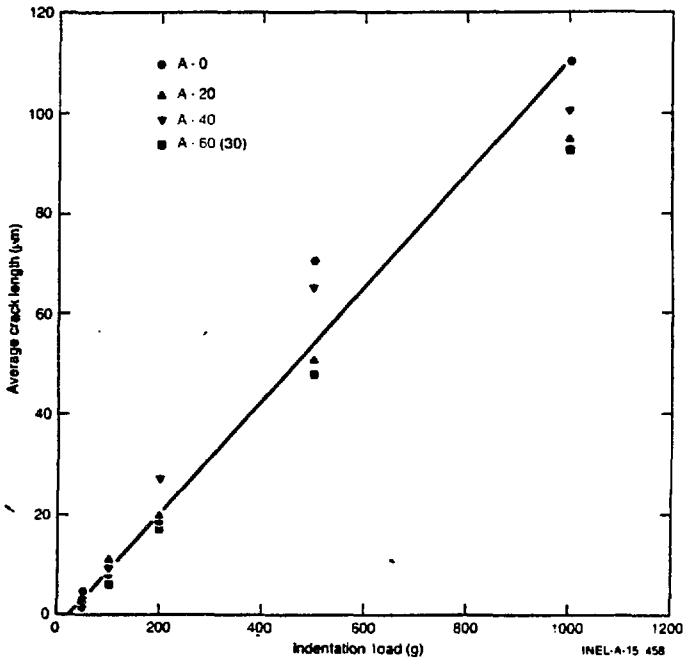

Figure 2. Indentor load effect on average crack length.

The results and discussion on the durability observations, i.e., leaching and mechanical properties, strongly suggest that controlled cooling of the melts to promote more devitrification should be explored. This approach would reduce the amount of glass phase as well as minimize microcracking.

SUMMARY AND FUTURE CONSIDERATIONS

The electromelt process and the resulting iron-rich castings offer great promise for rendering nuclear waste into a stable form. The process offers great flexibility with regard to both compositional variation of the incoming waste and the high rates at which the waste can be introduced and cast. The cast product, a fine-grained basalt-like material, shows excellent homogeneity with little or no reaction to the steel containment. The preliminary mechanical and chemical durability data show the form to have adequate containment properties for TRU waste. However, work presently underway to improve these properties through additives and controlled cooling cycles has greatly enhanced the durability of the waste form. Furthermore, recent evidence indicates that divalent iron (Fe^{2+}) included in the crystalline phases of granites and basalts imparts a resistance to leaching[3] of uranium and other actinide ions[4,5]. The mechanism for this resistance is believed to

be the Fe^{2+}/Fe^{3+} buffer system which prevents oxidation of actinides in the waste form and inhibits reactions with carbonate and sulfate complexes in the ground water.

The flexibility of the electromelt process, combined with the potential superior durability of the iron-enriched synthetic basalt, indicate that this waste form system should be considered for all types (high level and low level) of nuclear waste consolidation and containment.

REFERENCES

1. N. D. Cox et al., Figure-of-Merit Analysis for TRU Waste Processing Facility at INEL, TREE-1293, EG&G Idaho, Inc., October 1978.
2. J. E. Flinn et al., Summary of FY-1979 Material Support Studies for SPI - Migration and Immobilization, EGG-FM-5041, EG&G Idaho, Inc., September 1979.
3. J. A. Speer, T. Soldberg, and S. W. Becker, "Petrography of U-Bearing Minerals of the Liberty Hill Pluton, South Carolina: Phase Assemblages and Migration of U in Granitoid Rocks," unpublished manuscript.
4. G. W. Beall, G. D. O'Kelley and B. Allard, "An Autoradiographic Study of Actinide Sorption of Climax Stock Granite," ORNL-5617, June 1980.
5. G. W. Bird, "Geochemistry of Radioactive Waste Disposal," Geoscience Canada 6: 199-204 (1980).

ACKNOWLEDGEMENT

This work was supported by the U. S. Deparment of Energy, Assistant Secretary for Nuclear Energy, Office of Waste Management, under DOE Contract No. DE-AC07-76ID01570